

The pure rotational spectrum and hyperfine structure of CF studied by laser magnetic resonance

Richard J. Saykally and Karen G. Lubic

Department of Chemistry, University of California, Berkeley, California 94720

Artemio Scalabrin^{a)} and Kenneth M. Evenson

Time and Frequency Division, National Bureau of Standards, Boulder, Colorado 80302

(Received 21 July 1981; accepted 2 March 1982)

Laser magnetic resonance spectra have been measured for four rotational transitions and one spin-changing transition in the $^2\Pi$ ground state of CF, generated in an intracavity methane-fluorine flame. From a detailed analysis of the Zeeman hyperfine structure of the $J = 9/2 \rightarrow 11/2$ transition in the $\Omega = 3/2$ spin component the hyperfine constants h , b , and d as well as B_0 and q_0 have been determined. Using these fitted parameters in conjunction with *ab initio* results, the values of $\langle 1/r^3 \rangle$, $\langle (3 \cos^2\theta - 1)/r^3 \rangle$, $|\psi^2(0)|$, and $\langle (\sin^2\theta)/r^3 \rangle$, averaged over the unpaired electron distribution, have been determined. Comparison of these integrals with those of the fluorine atom indicates that the unpaired electron has approximately 18% F character, implying a substantial degree of double bonding.

INTRODUCTION

The carbon-containing diatomics CH,¹ CN,² CO,³ CS,⁴ and CCl,⁵ recently have been studied by pure rotational spectroscopic techniques. Such experiments have provided precise information on the electronic structure and bonding in these simple molecules. Notably missing from the list is CF, the simplest fluorocarbon. In order to understand more generally the electronic properties of carbon-containing diatomics, we have studied the pure rotational spectrum of CF by the technique of far-infrared laser magnetic resonance.

Since the discovery of the CF B-X and A-X electronic transitions by Andrews and Barrow⁶ in 1950, electronic spectra of CF have been studied by several techniques, including flash photolysis, shock tube excitation, thermal decomposition, electrical discharges,⁷ and flame techniques. This work has revealed a complex structure of excited electronic states dominated by avoided crossings and heterogeneous perturbations. Recent theoretical efforts have succeeded fairly well in producing a qualitative understanding of the excited state structure, but the agreement with experimental measurements is far from precise. Aside from electronic spectroscopy, four experiments have been carried out on the ground $X^2\Pi$ state of CF. Jacox and Milligan⁸ detected the infrared spectrum in cryogenic matrices in 1969. Carrington and Howard⁹ observed the EPR spectrum of $J = 3/2$ and $J = 5/2$ levels of the $\Omega = 3/2$ spin component in a fluorine atom-hydrocarbon flame. Saykally and Evenson¹⁰ reported measurement of several pure rotational transitions of CF in a fluorine atom-methane flame for both $\Omega = 3/2$ and $\Omega = 1/2$ states, as well as transitions thought to occur between spin states. Most recently, Kawaguchi *et al.*¹¹ have reported observing CF vibrational and rotational spectra in ac discharges of C_2F_4 and CF_4 using diode lasers and micro-

wave spectroscopy. In this paper, we discuss the detection of the far-infrared laser magnetic resonance spectra and report a detailed analysis of the $J = 9/2 \rightarrow 11/2$ pure rotational Zeeman spectrum.

Analysis of the EPR spectra yielded experimental values for the effective g factors of the $J = 3/2$ and $J = 5/2$ states, the axial magnetic hyperfine interaction $h = a + (1/2)(b + c)$, and the isotropic hyperfine contribution b , where a , b , and c are the traditional Frosch and Foley¹² parameters. These constants were calculated by fixing the spin-orbit and rotational constants at values given by optical spectra. Carrington and Howard were also able to determine the permanent molecular dipole moment by applying static electric fields across the microwave cavity.⁹ Atomic orbital approximations were invoked to obtain estimates for the separate values of a , b , and c , which do not agree very well with the recent calculations of Hall and Richards¹³ made in the RHF approximation. Kawaguchi *et al.*¹¹ were able to extract B_e , α_e , D_e , the lambda doubling constants p_0 and p_1 , and the band center from a combined fit of the infrared and microwave data. The observation of hyperfine structure in the microwave spectra was reported but no analysis of hyperfine effects was given. We present here the values for B_0 , q_0 , h , b , and d , the hyperfine doubling interaction, obtained from a combined nonlinear least-squares analysis of 52 LMR and 12 EPR transitions.

EXPERIMENTAL

An energy level diagram for the $X^2\Pi$ state of CF is given in Fig. 1. Pure rotational transitions were predicted from the optical data of Porter, Mann, and Acquista⁷ with a simplified $X^2\Pi$ Hamiltonian. A search for several transitions predicted to be coincident with known FIR lasing transitions was carried out. A fluorine atom-methane flame was used as a source of CF radicals,¹⁰ having previously produced LMR spectra of CH,¹ CH₂,^{14,15} CCH,¹⁶ and CH₂F.¹⁷ A total of five LMR transitions in CF was detected.

^{a)} Present address: Instituto de Fisica, UNICAMP, Universidade Estadual de Campinas, 13100 Campinas, San Paulo, Brazil.

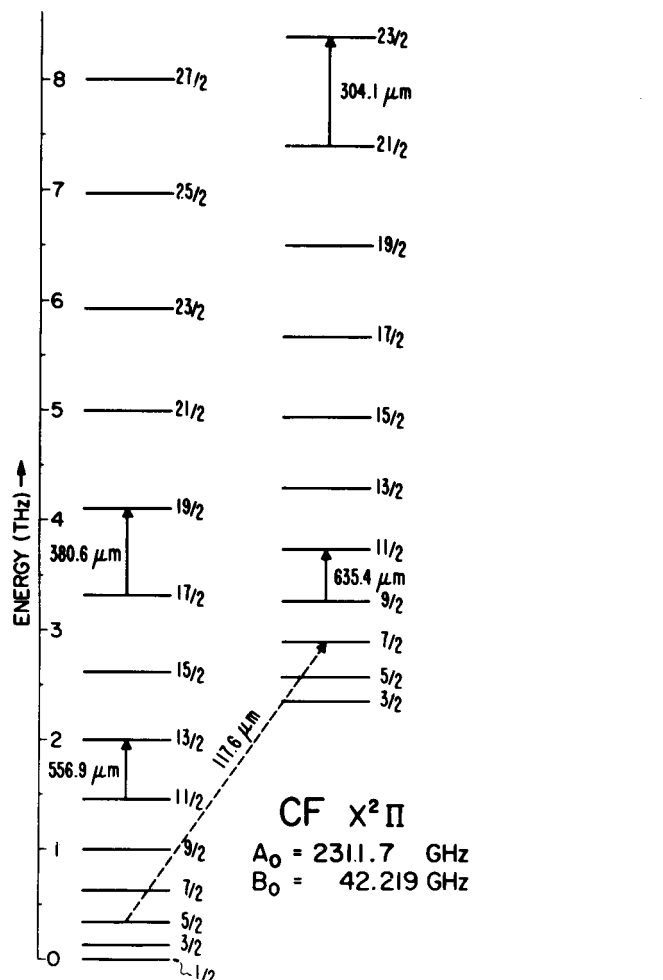


FIG. 1. Energy level diagram for $X^2\Pi$ CF, showing the observed transitions. The rotational constants are those of Porter, Mann, and Acquista (Ref. 7).

The LMR spectrometer used in this work at NBS-Boulder is diagrammed in Fig. 2. It consists of a far-infrared gain cell pumped transversely by a cw grating and piezoelectrically tuned CO_2 laser with a power output near 30 W on a single line, and an intracavity sample region, which is located between the pole faces of a

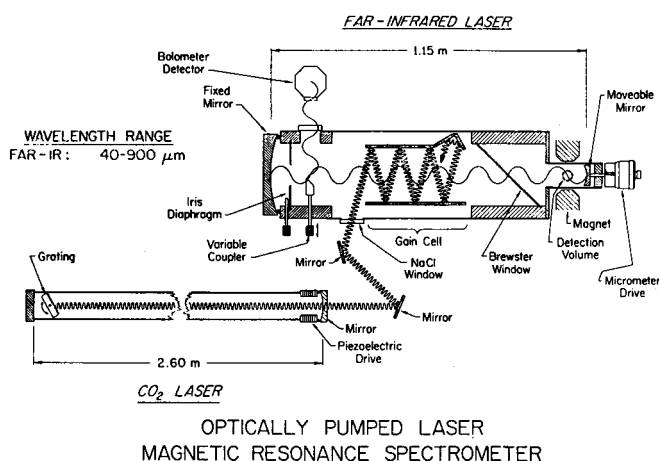


FIG. 2. Diagram of the laser magnetic resonance spectrometer.

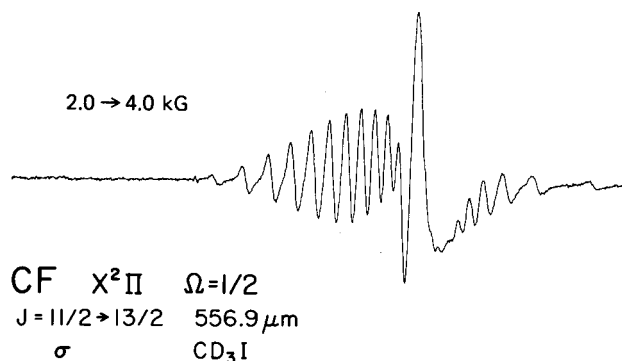


FIG. 3. The laser magnetic resonance spectrum of $X^2\Pi_{1/2}$ CF, $J=11/2-13/2$ using the $556.9 \mu\text{m}$ laser line of CD_3I pumped by the $10 P(36)$ line of CO_2 . The fluorine atom-methane flame composition was 0.1% $\text{CH}_4/1.6\% \text{F}_2/98.3\% \text{He}$.

37.5 cm electromagnet capable of reaching fields of 2.0 T. The gain cell and sample region are separated by a rotatable polypropylene beam splitter, which also determines the polarization (σ or π) of the laser electric field relative to the static magnetic field. Fluorine atoms, produced in a 2450 MHz discharge through a dilute (<1%) mixture of F_2 in He, flow down the inner tube of a concentric flow reactor extending to the perimeter of the laser cavity and mix with CH_4 , added through the outer tube, producing a bright, white flame in the homogeneous field region of the sample cavity. As a transition in CF is tuned into resonance with the FIR laser frequency, the total power oscillating inside the cavity changes and is modulated at 5 kHz by a set of Helmholtz coils. The output of the laser is coupled into a helium-cooled germanium bolometer by a 45° cylindrical mirror 6 mm in diameter, which is inserted optimum distance into the mode pattern. The output of the detector is preamplified and fed into a lock-in amplifier. The demodulated output signal, observed on an xy plotter, approximates the first-derivative of the absorption spectrum as a function of magnetic flux density.

The optimum fluorine atom-methane flame composition for the production of CF radicals was determined to be about 0.1% $\text{CH}_4/1.6\% \text{F}_2/98.3\% \text{He}$ at total pressures near 133 Pa (133 Pa = 1 Torr). This is considerably richer in fluorine atoms than the optimum flames used to generate CH^1 or CH_2^{15} spectra, and is slightly richer than that used for production of carbon atoms¹⁶ in the same system.

The transitions observed in this study and the FIR laser lines used to detect them are listed in Table I. Frequencies of the laser lines were taken from the tables of Knight¹⁸ and are considered accurate to $\pm 5 \times 10^{-7}$. Magnetic flux densities were measured with an NMR gaussmeter. Most lines below 1.5 T were measured with an accuracy of 3×10^{-4} T, while those at higher flux densities were accurate to $\pm 5 \times 10^{-3}$ T. The signs of the tunabilities ($\partial H/\partial \nu$) of observed transitions were determined by either red- or blue-shifting the FIR laser frequency by changing the cavity length and observing the corresponding change in the flux density.

The observed spectra are shown in Figs. 3-7. These

TABLE I. Observed LMR transitions and FIR laser lines used.

Transition	Laser medium	Laser λ (μm)	Laser ν (GHz)
$J=11/2 \rightarrow 13/2; \Omega=1/2$	CD ₃ I	556.9	538.3470
$J=17/2 \rightarrow 19/2; \Omega=1/2$	DCOOD	380.6	787.7555
$J=9/2 \rightarrow 11/2; \Omega=3/2$	CH ₂ CHBr	635.4 ^a	471.8505
$J=21/2 \rightarrow 23/2; \Omega=3/2$	DCOOD	304.1	985.8897
$J=5/2 \rightarrow 7/2; \Omega=1/2 \rightarrow 3/2$	CH ₂ F ₂	117.6 ^b	2447.9685

556.9 μm spectrum (All flux densities given in Gauss, $1\text{T}=10^4\text{G}$)

π	σ	σ	σ
2526.9	2129.0	3072.0	3540.4
2574.7	2557.2	3123.0	3609.3
2593.2	2619.1	3169.1	3712.1
2789.2	2724.4	3214.4	3897.6
8767.1	2812.8	3251.3	4949.2
8883.3	2888.5	3322.3	5160.1
8904.1	2889.0	3455.5	5308.9
12223.7	2955.9	3491.2	6721.1

380.6 μm spectrum

π No lines observed

σ	σ	σ	σ
13430	15650	16761	19206
13640	15687	17313	19242
13852	15814	17651	19429
14068	15861	17984	19531
14277	15955	18258	19656
14493	16052	18312	19811
14700	16109	18476	19871
14901	16230	18630	20083
15078	16377	18703	20315
15312	16560	18936	20500
15506	16574	18965	

304.1 μm spectrum

π	π	σ	σ	σ
2317.5	9949.1	1317.0	3500.0	15988.0
2563.2	10216.0	1413.6	3599.5	17367.0
2603.2	10676.0	1515.9	3760.2	17745.0
2864.5	13436.0	1663.3	3804.1	
3114.7	14037.0	1789.0	4009.0	
3177.0	17453.0	1856.3	4321.0	
3262.0	17999.0	1929.6	4484.3	
3325.4		1986.3	4542.4	
3427.8		2107.0	4702.7	
3586.8		2145.8	4996.0	
3678.0		2246.0	5223.3	
3781.3		2308.6	5530.0	
3846.2		2315.9	5694.8	
4105.9		2319.5	5896.9	
4151.0		2367.2	6129.0	
1352.0		2385.4	7143.6	
4481.0		2404.4	7237.8	
4660.2		2428.4	7448.7	
4866.0		2540.7	9231.2	
5028.1		2593.8	9359.7	
5375.6		2618.0	9429.4	
5514.9		2749.0	9507.4	
5925.2		2825.1	9964.0	
6344.2		2902.8	10133.0	
7165.0		2979.8	10829.0	
7304.0		3082.9	11918.0	
7608.5		3258.5	13296.0	
9517.5		3412.3	14781.0	

^aFlux densities given in Table II.

^bPrecise flux densities not yet available.

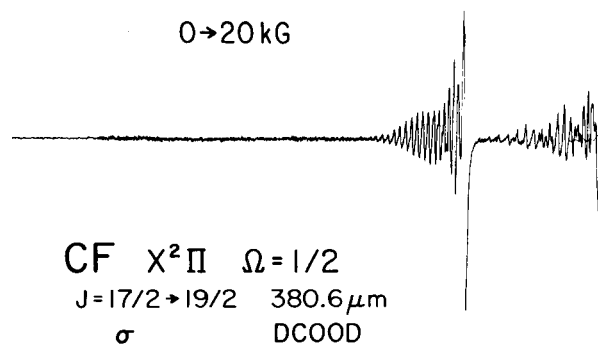


FIG. 4. The $J=17/2 \rightarrow 19/2$ spectrum of $X^2\Pi_{1/2}$ CF using the 380.6 μm line of DCOOD pumped by the 10 $R(12)$ CO₂ line. This spectrum was taken under the same flame conditions as Fig. 3.

are low-resolution survey scans over the entire range of accessible magnetic flux densities 0.0–2.0 T. Figure 5 gives both the σ and π polarizations of the $J=9/2 \rightarrow 11/2$ transition in the $\Omega=3/2$ state observed with the 635.4 μm laser line of CH₂CHBr. This is the only “well-behaved” spectrum that was observed in this study, as is evident from the spectra in Figs. 3, 4, 6, and 7. The rest are rather badly overlapped or consist of large numbers of lines in irregular patterns. These latter transitions correspond to those predicted to lie in high- J levels (Figs. 3, 4, and 6) or to occur between the two spin states (Fig. 7) with $\Delta\Omega \neq 0$ selection rules that are weakly allowed because of the rotational distortion perturbation. In this particular case, three different transitions could possibly be observed with the same laser line. The intensities of all the spectral lines peaked under the same flame conditions given above and possessed high absolute intensities relative to other species known to be present under these conditions, viz., CH⁺, CH₂, CCH, CH₂F, carbon atoms, and OH. Only the 635.4 μm spectrum was easily assignable, consisting of nicely resolved sequences of

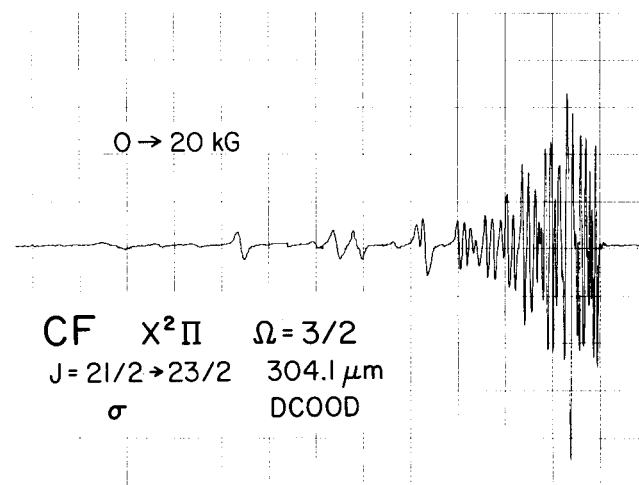


FIG. 5. The $J=21/2 \rightarrow 23/2$ spectrum of $X^2\Pi_{3/2}$ CF. This spectrum was observed with the 304.1 μm line of DCOOD, pumped by the 10 $R(24)$ CO₂ laser line. Flame conditions are given in Fig. 3.

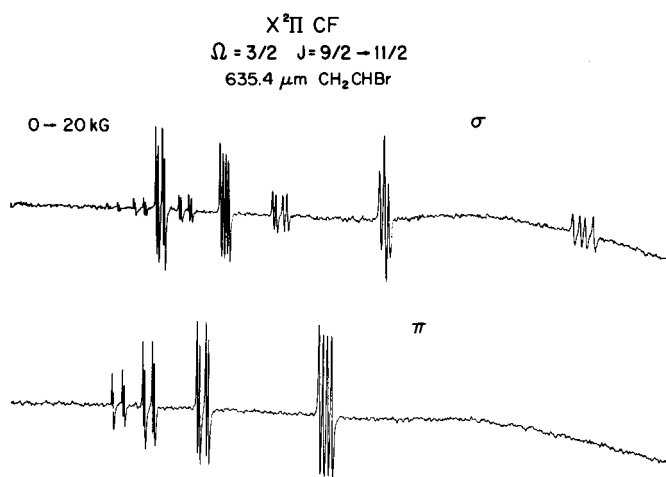


FIG. 6. Both σ and π spectra of $J = 9/2 \rightarrow 11/2$, $X^2\Pi_{3/2}$ CF. These spectra were taken with the 635.4 μm line of CH_2CHBr pumped by 10 $R(26)$ CO_2 line. Conditions were the same as Fig. 3.

doublets. By obtaining a detailed analysis of this transition, we sought to make some progress with the others.

THEORY

In order to predict, analyze, and interpret laser magnetic resonance rotational spectra of $^2\Pi$ states with a precision equal to that of experimental measurements, we have written a computer program based on the effective Hamiltonian approach of Brown *et al.*, which is discussed in detail in Eq. (19). Briefly, the total effective Hamiltonian has the form

$$H_{\text{eff}} = H_{\text{SO}} + H_{\text{ROT}} + H_{\text{CD}} + H_{\text{LD}} + H_{\text{HFS}} + H_Z. \quad (1)$$

Here, H_{SO} is the spin-orbit term; H_{ROT} gives the nuclear rotational energy; H_{CD} is the centrifugal distortion terms; H_{LD} represents the Lambda-doubling; and H_Z is the Zeeman term. Hund's case (a) notation is used for the explicit forms of these various contributions. The spin-orbit Hamiltonian is simply:

$$H_{\text{SO}} = A T_{q=0}^1(\mathbf{L}) T_{q=0}^1(\mathbf{S}), \quad (2)$$

where A is the spin-orbit constant. The rotational contribution is

$$H_{\text{ROT}} = B T^1(\mathbf{R}) \cdot T^1(\mathbf{R}) \equiv B R^2, \quad (3)$$

where $\mathbf{R} = \mathbf{J} - \mathbf{L} - \mathbf{S}$ and B is the rotational constant. Centrifugal distortion is given by

$$H_{\text{CD}} = -D(R^2)^2, \quad (4)$$

where only the quartic centrifugal distortion constant is used. The lambda-doubling term is

$$H_{\text{LD}} = \sum_{q'=\pm 1} \exp(-2iq'\phi) \times [-qT_{2q'}^2(\mathbf{J}, \mathbf{J}) + (p + 2q)T_{2q'}^2(\mathbf{J}, \mathbf{S})], \quad (5)$$

where p and q are the lambda-doubling parameters and ϕ is the electron orbital azimuthal coordinate. The nuclear hyperfine contribution is

$$H_{\text{HFS}} = a T_{q=0}^1(\mathbf{I}) T_{q=0}^1(\mathbf{L}) + b_F T^1(\mathbf{I}) \cdot T^1(\mathbf{S}) + \frac{c}{3} \sqrt{6} T_{q=0}^2(\mathbf{I}, \mathbf{S}) + d \sum_{q=\pm 1} \exp(-2iq\phi) T_{2q}^2(\mathbf{I}, \mathbf{S}). \quad (6)$$

Here a , c , and d are the traditional Frosch and Foley¹² hyperfine constants while b_F includes only the Fermi contact contribution to the Frosch and Foley b constant [$b_F = b + \frac{1}{3}c$]. The Zeeman Hamiltonian has the explicit form

$$H_Z = g_S \mu_B B_0 T_{p=0}^1(\mathbf{S}) + g'_L \mu_B B_0 T_{p=0}^1(\mathbf{L}) - g_r \mu_B B_0 T_{p=0}^1(\mathbf{J} - \mathbf{L} - \mathbf{S}) + g_I \mu_B B_0 \sum_{q=\pm 1} D_{0q}^{(1)}(\omega) * T_q^1(\mathbf{S}) - g_N \mu_N B_0 T_{p=0}^1(\mathbf{I}), \quad (7)$$

where g_S is the electron spin g factor, corrected for relativistic effects; g'_L is the electron orbital g factor, also corrected for relativistic effects; g_r is the rotational g factor; g_I represents the anisotropic corrections to the electron spin g factor; and g_N is the nuclear spin g factor. Also, μ_B is the Bohr magneton; μ_N is the nuclear magneton; and B_0 is the magnetic flux density.

The matrix elements, resulting from this Hamiltonian operating on a Hund's case (a) decoupled basis set, are given explicitly by Brown *et al.*¹⁹ for OH and are not listed here. By adopting Brown's use of parity as a good quantum number, the following expression, which was used in the actual computer programming of the matrix elements, is produced:

$$\langle J' M'_J \Omega' \pm | H | J M_J \Omega \pm \rangle = \langle \Lambda \Sigma J' M'_J \Omega' | H | \Lambda \Sigma J M_J \Omega \rangle \pm (-1)^{J-S} \langle \Lambda \Sigma J' M'_J \Omega' | H | -\Lambda \Sigma -J M_J -\Omega \rangle. \quad (8)$$

Here, s refers to Σ states and is even or odd depending on whether the state is Σ^+ or Σ^- . The second term in the above expression will be nonzero only for terms in the effective Hamiltonian, where q has the values ± 1 . This includes the lambda-doubling term and the part of the hyperfine term which involves the constant d (hyperfine doubling).

The molecular constants used in the matrix elements

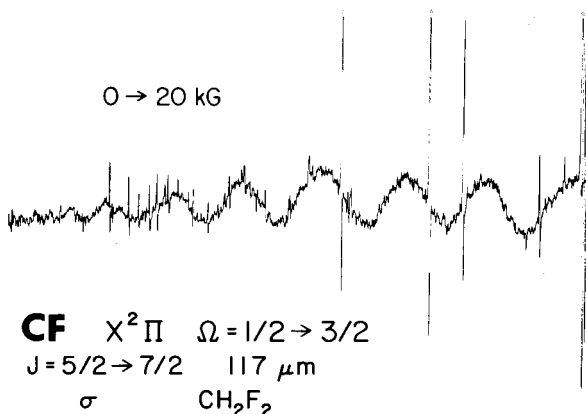


FIG. 7. The $J = 5/2 \rightarrow 7/2$, cross-spin spectrum of CF. This spectrum was observed with the 117 μm line of CH_2F_2 pumped by the 9 $R(20)$ CO_2 line. Flame conditions are given in Fig. 3. Strong lines marked with an asterisk are due to CH ($J = 5/2 \rightarrow 7/2$).

have retained their traditional definitions, except for the lambda-doubling parameters and some of the g factors. The lambda-doubling parameters p and q are the sum of second and third order perturbation contributions, with the second order terms being the same as those of Mulliken and Christy,²⁰ viz.

$$p^{(2)} = -4 \sum_{n'} (E_{n\pi} - E_{n'\sigma})^{-1} (-1)^s \times \langle n, \Lambda = 1 | AT_1^1(\mathbf{L}) | n', \Lambda = 0 \rangle \langle n', \Lambda = 0 | BT_{-1}^1(\mathbf{L}) | n, \Lambda = 1 \rangle,$$

$$q^{(2)} = 4 \sum_{n'} (E_{n\pi} - E_{n'\sigma})^{-1} (-1)^s \times | \langle n, \Lambda = 1 | BT_1^1(\mathbf{L}) | n', \Lambda = 0 \rangle |^2. \quad (9)$$

The g factors have the following definitions:

$$g'_L = g_L + \Delta g_L, \quad (10)$$

where the second term is the anisotropic orbital correction factor;

$$\Delta g_L = 2(g_L + g_r^N) \sum_{q=\pm 1} \sum_{n'\Lambda'} q(E_{n\pi} - E_{n'\Lambda'})^{-1} \times \langle n\Lambda | T_q^1(\mathbf{L}) | n'\Lambda' \rangle \langle n'\Lambda' | BT_{-q}^1(\mathbf{L}) | n\Lambda \rangle / \Lambda; \quad (11)$$

$$g_r = g_r^N - g_r^e, \quad (12)$$

where g_r^e is the electronic contribution to the rotational g factor;

$$g_r^e = 2(g_L + g_r^N) \sum_{q=\pm 1} \sum_{n'\Lambda'} (E_{n\Lambda} - E_{n'\Lambda'})^{-1} \times \langle n\Lambda | T_q^1(\mathbf{L}) | n'\Lambda' \rangle \langle n'\Lambda' | BT_{-q}^1(\mathbf{L}) | n\Lambda \rangle. \quad (13)$$

Finally, we have

$$g_I = -(g_L + g_r^N) \sum_{q=\pm 1} \sum_{n'\Lambda'} (E_{n\Lambda} - E_{n'\Lambda'})^{-1} \times \langle n\Lambda | T_q^1(\mathbf{L}) | n'\Lambda' \rangle \langle n'\Lambda' | AT_{-q}^1(\mathbf{L}) | n\Lambda \rangle. \quad (14)$$

ASSIGNMENT AND ANALYSIS OF THE 635.4 μm SPECTRUM

As we have noted before,²¹ most of the general features of an LMR pure rotational spectrum can be predicted from simple first-order expressions for the Zeeman and hyperfine perturbations. This situation, however, does not apply to transitions between states with very small g factors or to transitions which decouple easily in a magnetic field. In these cases, more sophisticated techniques must be applied. In the case of the 635.4 μm spectrum, such a simple treatment led to the assignments given in Table II.

A nonlinear least-squares fit of the 64 LMR and EPR transition frequencies at the observed flux densities was performed. The transition frequencies were determined by diagonalizing a 12×12 matrix for each M_J and parity at every magnetic flux density observed, including terms off-diagonal in J by one unit. The EPR and LMR transitions were weighted equally, but transitions occurring at flux densities exceeding 1.8 T were weighted by 1/400 since these could not be measured accurately. Three iterations resulted in convergence of nearly all transitions to within experimental error of

the observed frequencies, as shown in Table II. The values of the parameters determined in the analysis and their correlation matrix are given in Table III, compared with results from previous studies.

From the combination of LMR and EPR data, the set of constants B_0 , q_0 , h_0 , b_0 , and d_0 was determined. Initial values for these constants, as well as for others held fixed in the fit, were obtained from EPR data, optical and infrared spectra, or were calculated. Carington and Howard's⁹ hyperfine constants were used while the spin-orbit and rotational constants were taken from Porter, Mann, and Acquista's optical results.⁷ The centrifugal distortion term and lambda-doubling parameter p_0 were taken from Kawaguchi *et al.*¹¹ The g factors used in the Zeeman term of the Hamiltonian and given in Table IV, were calculated in the following ways. The orbital g factor (g'_L) is given by Abragam and van Vleck²² as

$$g'_L = 1.0 + \langle \delta g_I \rangle_{av} + \langle \delta g_I \rangle_{av} + \Delta g_L, \quad (15)$$

where

$$\langle \delta g_I \rangle_{av} = - \frac{1}{2m^2 c^2} \sum_i \left(\frac{\mathbf{p}^2}{L_z} \right) l_{iz} \quad (\text{relativistic correction}) \quad (16)$$

and

$$\langle \delta g_I \rangle_{av} = - \frac{e}{2mcL_z} \sum_{j \neq i} [(\mathbf{r}_i \times \mathbf{p}_j) \gamma_{ij}^{-1}]_z + [\gamma_{ij}^{-3} (\mathbf{r}_i \times \mathbf{r}_{ij}) (\mathbf{r}_{ij} \cdot \mathbf{p}_j)]_z \quad (\text{orbit-orbit correction}). \quad (17)$$

The calculation of $\langle \delta g_I \rangle_{av}$ may be done simply by assuming that the largest contribution comes from motion of π^* electrons of the fluorine atom near the fluorine nucleus. The equation for $\langle \delta g_I \rangle_{av}$ may be rewritten as²²

$$\langle \delta g_I \rangle_{av} = \frac{\langle T \rangle_{av}}{mc^2} [m_I + \frac{1}{5} m_s (8 - 2m_I^2)] \quad (18)$$

summed over the valence electrons. For a fluorine atom this reduces to

$$\langle \delta g_I \rangle_{av} = - \langle T \rangle_{av} / mc^2. \quad (19)$$

To calculate the kinetic energy of a π^* electron for CF, it was assumed to be the same as that of a p electron in a fluorine atom. Then²²

$$\langle T \rangle_{av} \equiv \frac{\hbar^2}{2m} \int \psi_{2p}^* \nabla^2 \psi_{2p} d\tau, \quad (20)$$

where Slater's hydrogenlike wave functions for the fluorine atom have been used. The final result is $\langle \delta g_I \rangle_{av} = -1.8 \times 10^{-4}$. A value for $\langle \delta g_I \rangle_{av}$ has not been calculated, since it is immeasurably small for most molecules. For $\text{O}_2(^1\Delta)$, Miller²³ estimated it to be -4×10^{-6} and Abragam and van Vleck²² calculate $\langle \delta g_I \rangle_{av}$ for atomic oxygen to be -3.1×10^{-5} . The value of Δg_L was also determined to be about 10^{-5} and therefore was not included in g'_L .

In determining g_r , both nuclear and electronic contributions must be calculated. The nuclear part is²⁴

$$\langle n | g_r^N | n' \rangle = m \sum_{\alpha} \left\langle n \left| \frac{Z_{\alpha} \mathbf{r}_{\alpha}^2}{I} \right| n' \right\rangle \quad (21)$$

summed over the number of nuclei α .

TABLE II. Frequencies and flux densities for CF in $X^2\Pi$ ground state.

J''	J'	M_J''	M_J'	M_L''	M_L'	Parity of lower state	Flux density (G)	ν_{obs} (MHz)	ν_{calc} (MHz)	$\nu_{\text{obs}} - \nu_{\text{calc}}$ (MHz)	Weight
9/2	11/2	9/2	9/2	1/2	1/2	+	3 028.3	471 850.50	471 850.09	0.41	1
9/2	11/2	9/2	9/2	1/2	1/2	-	3 066.5		471 850.34	0.16	1
9/2	11/2	9/2	9/2	-1/2	-1/2	+	3 345.0		471 850.60	-0.10	1
9/2	11/2	9/2	9/2	-1/2	-1/2	-	3 393.4		471 850.99	-0.49	1
9/2	11/2	7/2	7/2	1/2	1/2	+	3 962.9		471 850.28	0.22	1
9/2	11/2	7/2	7/2	1/2	1/2	-	4 015.8		471 850.53	-0.03	1
9/2	11/2	7/2	7/2	-1/2	-1/2	+	4 242.4		471 850.46	0.04	1
9/2	11/2	7/2	7/2	-1/2	-1/2	-	4 303.1		471 850.75	-0.25	1
9/2	11/2	5/2	5/2	1/2	1/2	+	5 598.4		471 850.31	0.19	1
9/2	11/2	5/2	5/2	1/2	1/2	-	5 673.8		471 850.65	-0.15	1
9/2	11/2	5/2	5/2	-1/2	-1/2	+	5 859.5		471 850.47	0.03	1
9/2	11/2	5/2	5/2	-1/2	-1/2	-	5 942.0		471 850.75	-0.25	1
9/2	11/2	3/2	3/2	1/2	1/2	+	9 309.0		471 850.35	0.15	1
9/2	11/2	3/2	3/2	1/2	1/2	-	9 434.3		471 850.71	-0.21	1
9/2	11/2	3/2	3/2	-1/2	-1/2	+	9 561.1		471 850.39	0.11	1
9/2	11/2	3/2	3/2	-1/2	-1/2	-	9 691.0		471 850.74	-0.24	1
9/2	11/2	9/2	7/2	1/2	1/2	+	2 281.7	471 850.50	471 850.90	-0.40	1
9/2	11/2	9/2	7/2	1/2	1/2	-	2 302.8		471 851.19	-0.69	1
9/2	11/2	9/2	7/2	-1/2	-1/2	+	2 664.3		471 851.55	-1.05	1
9/2	11/2	9/2	7/2	-1/2	-1/2	-	2 707.2		471 851.90	-1.40	1
9/2	11/2	7/2	5/2	1/2	1/2	+	2 850.5		471 851.24	-0.74	1
9/2	11/2	7/2	5/2	1/2	1/2	-	2 883.4		471 851.51	-1.01	1
9/2	11/2	7/2	5/2	-1/2	-1/2	+	3 172.2		471 851.62	-1.12	1
9/1	11/2	7/2	5/2	-1/2	-1/2	-	3 222.1		471 851.97	-1.47	1
9/2	11/2	5/2	3/2	1/2	1/2	+	3 663.0		471 851.57	-1.06	1
9/2	11/2	5/2	3/2	1/2	1/2	-	3 707.3		471 851.90	-1.40	1
9/2	11/2	5/2	3/2	-1/2	-1/2	+	3 962.8		471 851.94	-1.44	1
9/2	11/2	5/2	3/2	-1/2	-1/2	-	NA		NA	NA	1
9/2	11/2	9/2	11/2	1/2	1/2	+	4 331.5		471 848.83	1.67	1
9/2	11/2	9/2	11/2	1/2	1/2	-	4 399.4		471 849.19	1.31	1
9/2	11/2	9/2	11/2	-1/2	-1/2	+	4 531.9		471 848.75	1.75	1
9/2	11/2	9/2	11/2	-1/2	-1/2	-	4 586.9		471 849.14	1.36	1
9/2	11/2	3/2	1/2	1/2	1/2	+	5 029.7	471 850.50	471 852.18	-1.68	1
9/2	11/2	3/2	1/2	1/2	1/2	-	5 093.0		471 852.43	-1.93	1
9/2	11/2	3/2	1/2	-1/2	-1/2	+	5 325.7		471 852.42	-1.92	1
9/2	11/2	3/2	1/2	-1/2	-1/2	-	5 408.1		471 852.72	-2.22	1
9/2	11/2	7/2	9/2	1/2	1/2	+	6 280.0		471 848.05	2.45	1
9/2	11/2	7/2	9/2	1/2	1/2	-	6 373.0		471 848.32	2.18	1
9/2	11/2	7/2	9/2	-1/2	-1/2	+	6 461.6		471 849.87	2.63	1
9/2	11/2	7/2	9/2	-1/2	-1/2	-	6 538.9		471 848.36	2.14	1
9/2	11/2	1/2	-1/2	1/2	1/2	+	7 873.4		471 853.17	-2.67	1
9/2	11/2	1/2	-1/2	1/2	1/2	-	7 974.3		471 853.43	-2.93	1
9/2	11/2	1/2	-1/2	-1/2	-1/2	+	8 148.0		471 853.47	-2.97	1
9/2	11/2	1/2	-1/2	-1/2	-1/2	-	8 310.1		471 853.74	-3.24	1
9/2	11/2	5/2	7/2	1/2	1/2	+	11 137.9		471 846.33	4.18	1
9/2	11/2	5/2	7/2	1/2	1/2	-	11 284.6		471 847.15	3.35	1
9/2	11/2	5/2	7/2	-1/2	-1/2	+	11 284.6		471 845.72	4.78	1
9/2	11/2	5/2	7/2	-1/2	-1/2	-	11 404.0		471 846.79	3.71	1
9/2	11/2	-1/2	-3/2	1/2	1/2	+	18 004.0		471 814.75	35.75	1/400
9/2	11/2	-1/2	-3/2	1/2	1/2	-	18 202.0		471 815.85	34.66	1/400
9/2	11/2	-1/2	-3/2	-1/2	-1/2	+	18 338.0		471 817.17	33.33	1/400
9/2	11/2	-1/2	-3/2	-1/2	-1/2	-	18 604.0		471 817.06	33.44	1/400
3/2	3/2	-3/2	-1/2	1/2	1/2	+	8 623.4	9 270.22	9 268.97	1.25	1
3/2	3/2	-3/2	-1/2	-1/2	-1/2	+	8 859.8		9 268.52	1.70	1
3/2	3/2	-1/2	1/2	1/2	1/2	+	8 496.8		9 268.51	1.71	1
3/2	3/2	-1/2	1/2	-1/2	-1/2	+	8 740.2		9 269.00	1.22	1
3/2	3/2	1/2	3/2	1/2	1/2	+	8 367.6		9 268.36	1.86	1
3/2	3/2	1/2	3/2	-1/2	-1/2	+	8 617.5		9 268.24	1.98	1
5/2	5/2	-1/2	1/2	1/2	1/2	+	21 129.2		9 269.09	1.13	1
5/2	5/2	-1/2	1/2	-1/2	-1/2	+	21 382.4		9 267.74	2.48	1
5/2	5/2	-3/2	-1/2	1/2	1/2	+	20 330.6		9 263.99	6.23	1
5/2	5/2	-3/2	-1/2	-1/2	-1/2	+	20 581.8		9 264.20	6.02	1
5/2	5/2	-5/2	-3/2	1/2	1/2	+	19 794.9		9 269.65	0.57	1
5/2	5/2	-5/2	-3/2	-1/2	-1/2	+	20 042.2		9 271.11	-0.89	1

TABLE III. Molecular parameters for the $X^2\Pi$ CF ground state of CF.

Parameter	This work	Standard error ^b	Carrington and Howard ^c	Kawaguchi <i>et al.</i> ^d
A	2.31×10^6 ^a	F		
B_0	42196.35	2.80×10^{-2}	42218.88	42196.45 (0.63)
D	0.199	F		0.199 (0.004)
P_0	257.22	F		257.22 (0.63)
q_0	0.83	0.19		
A_D	-6.36	F		-6.36 (0.60)
b	253	22.0	190.0 (50)	
d	782	309.0		
h	665.7	8.3	662.9 (3.0)	

All values given in MHz

Correlation matrix

	B_0	h	b	d	q
B_0	1.00	0.11	-0.09	0.02	0.03
h		1.00	-0.92	-0.04	0.02
b			1.00	0.05	-0.02
d				1.00	0.11
q					1.00

Standard deviation of fit = 2.17 MHz

^aValue determined by Porter, Mann, and Acquista (Ref. 7).

^b F implies parameter fixed at appropriate value in table.

^cReference 9.

^dReference 11.

Here, m is the mass of electron; I is the moment of inertia; Z_α is the nuclear charge; \mathbf{r}_α is the distance from center of mass to nucleus α ; and n denotes an electronic state. Assuming only diagonal matrix elements, $g_r^N = 2.7 \times 10^{-4}$. In order to calculate g_r^e , we used Eq. (13) and assumed van Vleck's hypothesis of pure precession. Since, for a $^2\Pi$ state an adjacent $^2\Sigma$ state will give the largest interaction,

$$g_r^e = 2B(g_L + g_r^N)(E_{2\Pi} - E_{2\Sigma})^{-1} \times \langle ^2\Pi | T_1^1(\mathbf{L}) | ^2\Sigma \rangle \langle ^2\Sigma | T_{-1}^1(\mathbf{L}) | ^2\Pi \rangle. \quad (22)$$

This gives $g_r^e = 6.6 \times 10^{-5}$ which then yields $g_r = 2.0 \times 10^{-4}$. To calculate g_l , Eq. (14) was used and again pure precession was invoked. This gave $g_l = -1.81 \times 10^{-3}$. Finally for g_s , only a relativistic correction was made to the free electron value according to $g_s = g_s(\text{free electron}) + g_s(\text{free electron})(\delta g_l)_{av}$. This gave $g_s = 2.00196$.

RESULTS AND DISCUSSION

From Table III we see that B_0 , h_0 , and b_0 are determined rather well in this analysis, while the values obtained for q and d are considerably less precise. The fitted value of B_0 is about 0.10 MHz less than that determined by Kawaguchi *et al.*¹¹ and is roughly five times as precise. The axial hyperfine interaction h is in excellent agreement (within 0.3%) with Carrington and Howard's⁹ determination, but the value we obtain for the isotropic contribution b is just outside of their

quoted error limits. In their experiment they were limited by sampling only the $J=3/2$ and $J=5/2$ rotational states, which couple approximately according to case (a). In a pure case (a) state only the axial hyperfine interaction $a + 1/2(b + c)$ can be measured in an EPR experiment. In the case of CF the nonaxial hyperfine component (b) was sampled indirectly through the rotational mixing of $\Omega = 1/2$ wave functions with the $\Omega = 3/2$ levels, which is rather small for the low- J states observed. Consequently, the value of b derived from EPR measurements was not well determined. Since our analysis includes the $J=9/2$ and $J=11/2$ states, as well as Carrington and Howard's EPR measurements, we determine this interaction more precisely.

Carrington and Howard⁹ were able to make some interesting qualitative deductions from their data regarding the hybridization in CF and the s and p character of the molecular orbitals containing the unpaired electron, but these arguments were based on necessarily crude

TABLE IV. g Factors for CF in the $X^2\Pi_{3/2}$ ground state.

g_l	0.99989
g_s	2.00196
g_l	-1.81×10^{-3}
g_r	2.0×10^{-4}

assumptions and cannot be expected to be precise. Hall and Richards¹³ have since carried out *ab initio* calculations on the ground state of CF in the RHF approximation. We compare our results in Table V. Their quoted value of 522 MHz for h is 22% lower than ours, while their given value for b is 58% smaller. The large discrepancy in the isotropic term is rather predictable since in the RHF approximation the unpaired electron in the antibonding $^2\pi$ orbital cannot have any s character and, hence, can have no Fermi contact interaction. Hall and Richards¹³ calculate a value of -318 MHz for the spin-spin dipolar term c , compared with the estimate of -486 MHz from Carrington and Howard.⁹ Since h and b are directly determined in our analysis, we need only employ the RHF calculation of c , which we could not determine from our data, in order to check the consistency of the RHF results. If we use for c the value -318 MHz, we obtain for $a = h - 1/2(b + c)$ and $b_F = b + 1/3c$ the results 698 and 147 MHz, respectively.

The agreement between our calculated value of a and the theoretical result indicates that the RHF calculation of a and c are reliable to about 10%. Therefore, we obtain as the present best estimates of the individual hyperfine terms our values in Table V. We return our experimental value of d even though it is not determined well. If one assumes that value of $\langle 1/r^3 \rangle$ is the same for both the spin and orbital parts of the hyperfine interaction, then the following relation holds:

$$c = 3(a - d). \quad (22)$$

With Eq. (22) we obtain a RHF value of $d = 804$ MHz, which agrees well within the estimated precision of these calculations. Using our constants from Table V in Eq. (22) we calculate $c = -252$ MHz, whereas the RHF result is -318 MHz. For the isoelectronic molecule ^{14}NO , this formula predicts $c = -84.8$ MHz, while the true value is -58.13 MHz,²⁵ which is about the same level of agreement.

Kawaguchi's value of 257.2 MHz for p can be combined with results calculated in the pure precession approximation to yield some insights into the electronic structure of CF. From the definition of p given in Eq. (14) and the pure precession results

$$\begin{aligned} \langle \Lambda = 1 | AT_1^z(\mathbf{L}) | A = 0 \rangle &= -A, \\ \langle \Lambda = 1 | BT_1^z(\mathbf{L}) | \Lambda = 0 \rangle &= -B, \end{aligned} \quad (23)$$

we obtain the simple expression

TABLE V. Individual hyperfine parameters for CF. All values in MHz.

	This work	Carrington and Howard ^a	Hall and Richards ^b
a	698	812	628
b	253	190	106
c	-318	-486	-318
b_F	147	28	0
d	782		
h	665.7	662.9	522

^aReference 9.

^bReference 13.

TABLE VI. Magnetic hyperfine structure parameters for CF, NO, and F-atom. All values in cm^{-3} . The conversion factor used is $\mu_0 \mu_B = 7.0689 \times 10^{-24} \text{ cm}^3 \text{ MHz}$.

	CF	NO ²⁵	F ²⁸
$\langle \frac{1}{r^3} \rangle \times 10^{-24}$	9.40	14.76	51.15
$\psi^2(0) \times 10^{-24}$	0.236	0.46	0.49
$\langle \frac{3 \cos^2 \theta - 1}{r^3} \rangle \times 10^{-24}$	-2.85	-6.79	
$\langle \frac{\sin^2 \theta}{r^3} \rangle \times 10^{-24}$	7.02	13.16	

$$p = \frac{4AB(-1)^s}{|\Delta E_{\pi\pi}|}. \quad (24)$$

Inserting the values of A and B from Table III, we calculate a value for the separation of the $X^2\Pi$ and perturbing $^2\Sigma$ state of 6.3 eV. Furthermore, the positive sign of p implies that the perturbing state has Σ^- symmetry. Dunning *et al.*²⁶ have calculated the potential energy curves for the low-lying repulsive $^2\Sigma$ states of CF. For the lowest $^2\Sigma^-$ state, $|E_{\pi\pi}|$ at the r -centroid point for the two "precessing" electronic states is even greater than that for $A^2\Sigma^+$. Therefore, for pure precession, the A state would be expected to be the perturbing Σ state, except that it has incorrect Krönig symmetry.

This leads to the conclusion that pure precession does not hold for CF. This is not surprising since Mulliken and Christy²⁰ pointed out and Hinkley *et al.*²⁷ calculated that pure precession will only work well for molecules which approach the united atom limit; that is, Λ is determined by a single electron or a single hole. For example, in OH pure precession describes the Λ doubling quite well. For a molecule such as NO, this is not at all true. Pure precession fails to describe the Λ doubling correctly and the contributions from all Σ states must be included. In order to calculate p for CF correctly, then, all Σ states must be included, which is not practical since they are not all well characterized.

Finally, we shall discuss the information on the electronic structure of CF provided by the hyperfine analysis. The set of hyperfine constants in Table V was used to calculate the respective integrals over the unpaired electron density. In Table VI these integrals are compared with those in NO.²⁵ Generally, there is a decrease of 30%–70% in all of the CF averages relative to the NO values. In NO the $2p\pi$ molecular orbital of the unpaired electron is approximately 65% N in character, indicating that in CF both the contact interaction and the value of $\langle 1/r^3 \rangle$ for the fluorine nucleus should be smaller than for N in NO on the basis of the electron distribution.

Indeed, $\psi^2(0)$ for fluorine in CF has a value which is lower than that for nitrogen in NO and is a factor of two smaller than that in the fluorine atom.²⁸ This implies a significant amount of configuration mixing in the 2π antibonding orbital and indicates that a substantial re-

TABLE VII. Rotational energy levels of CF.

J	$\Omega = \frac{1}{2}$			$\Omega = \frac{3}{2}$		
	Parity	F	Energy (MHz)	Parity	F	Energy (MHz)
$\frac{1}{2}$	-	1	-1 071 217.54			
	+	1	-1 071 724.04			
	+	0	-1 071 739.35			
	-	0	-1 072 247.60			
$\frac{3}{2}$	+	2	-946 910.39	+	2	1 285 173.44
	-	2	-947 534.42	-	2	1 285 172.36
	+	1	-947 535.91	+	1	1 284 648.77
	-	1	-947 741.57	-	1	1 284 648.58
$\frac{5}{2}$	-	3	-739 786.80	-	3	1 500 051.17
	-	2	-740 330.88	+	3	1 500 047.25
	+	3	-740 636.74	-	2	1 499 721.96
	+	2	-740 895.33	+	2	1 499 720.34
$\frac{7}{2}$	+	4	-449 849.12	+	4	1 800 888.59
	+	3	-450 358.29	-	4	1 800 879.39
	-	4	-450 994.57	+	3	1 800 652.33
	-	3	-451 225.11	-	3	1 800 647.33
$\frac{9}{2}$	-	5	-77 096.33	-	5	2 187 631.30
	-	4	-77 588.19	+	5	2 187 613.75
	+	5	-78 434.90	-	4	2 187 450.61
	+	4	-78 727.60	+	4	2 187 439.68
$\frac{11}{2}$	+	6	378 485.22	+	6	2 660 222.66
	+	5	378 005.17	-	6	2 660 193.01
	-	6	376 894.12	+	5	2 660 079.43
	-	5	376 596.97	-	5	2 660 059.28
$\frac{13}{2}$	-	7	916 894.32	-	7	3 218 598.49
	-	6	916 420.03	+	7	3 218 552.68
	+	7	915 067.09	-	6	3 218 482.40
	+	6	914 766.35	+	6	3 218 449.46
$\frac{15}{2}$	+	8	1 538 153.98	+	8	3 862 686.49
	+	7	1 537 685.72	-	8	3 862 619.56
	-	8	1 536 074.88	+	7	3 862 591.11
	-	7	1 535 775.65	-	7	3 862 540.73
$\frac{17}{2}$	-	9	2 242 253.29	-	9	4 592 405.41
	-	8	2 241 786.96	-	8	4 592 326.28
	+	9	2 239 951.76	+	9	4 592 312.78
	+	8	2 239 651.84	+	8	4 592 254.39
$\frac{19}{2}$	+	10	3 029 224.38	+	10	5 407 667.12
	+	9	3 028 762.04	+	9	5 407 601.19
	-	10	3 026 673.43	-	10	5 407 542.63
	-	9	3 026 378.04	-	9	5 407 501.76
$\frac{21}{2}$	-	11	3 899 040.41	-	11	6 308 374.60
	-	10	3 898 578.51	-	10	6 308 319.40
	+	11	3 896 284.67	+	11	6 308 213.99
	+	10	3 895 989.40	+	10	6 308 188.49

arrangement of the fluorine electron density has occurred. The value of $\langle 1/r^3 \rangle$ for the fluorine atom is $51.2 \times 10^{24} \text{ cm}^{-3}$,²⁸ whereas for CF it is $9.40 \times 10^{24} \text{ cm}^{-3}$. If we represent the $2p\pi^*$ orbital as

$$\bar{\psi} = a_C \psi_{2p\pi}(C) + a_F \psi_{2p\pi}(F), \quad (25)$$

we find that $a_F^2 = 0.18$ and thus $a_F = 0.43$ and $a_C = 0.91$. Therefore, the unpaired electron can be viewed as spending about 18% of the time on fluorine. This is consistent with the Lewis structures $:\ddot{C}^- = \overset{+}{F}:$ and $\overset{-}{C} \equiv \overset{+}{F}:$ being admixed with the principal $\ddot{C} - \overset{-}{F}:$ configuration. It is interesting to note that the CF dipole moment measured by Carrington and Howard⁹ (0.65 ± 0.05) has been

shown theoretically to correspond to the polarity C^+F^- ,²⁶ in spite of the fact that the CF single bond is considered to be the most polar of any bond of carbon with a non-metal having 44% ionic character on the basis of electronegativity arguments,²⁹ with C^+F^- polarity. Both the bond length (1.2718 Å) and bond energy (130.4 kcal)³⁰ in the CF radical are indicative of substantial double bond character, compared to the average CF single bond length (1.38 Å) and energy (105.4 kcal).³¹ Furthermore, the hyperfine structure reflects the delocalization of the antibonding 2π orbital over both atoms. All of these features can be qualitatively rationalized from the generalized valence bond molecular orbital calculations of Dunning *et al.*²⁶ They show that the carbon $2p\pi$ bonding orbital is almost equally distributed between carbon and fluorine; the fluorine $2p\pi$ (1π) orbitals have delocalized onto carbon, and the carbon $2p\pi$ (2π) orbital has acquired substantial antibonding character. The carbon $2s$ (3σ) lobe functions, which contain the nonbonding electron pair, have rotated away from the fluorine atom. The combination of the 3σ carbon electrons being highly polarized and the back donation of electron density to the fluorine atom through the pi bonding overcomes the intrinsic C-F bond polarity and causes the observed dipole moment. A similar mechanism operates in the ground state of CO, in which the 5σ electrons localized on carbon cancel the CO bond polarity causing the very small dipole moment.³²

SUMMARY

From a detailed analysis of the Zeeman hyperfine structure of the $J=9/2 \rightarrow 11/2$ transition in the $\Omega=3/2$ spin component of the $^2\Pi$ ground state of CF, we have determined the hyperfine constants h , b , and d as well as B_0 and q_0 . Using these fitted hyperfine constants and an *ab initio* calculation of c the spin-spin dipolar interaction we have determined the other hyperfine parameters a and b_F . From these we have determined the values of

$$\langle 1/r^3 \rangle, \left\langle \frac{3 \cos^2 \theta - 1}{r^3} \right\rangle, \Psi^2(0), \text{ and } \left\langle \frac{\sin^2 \theta}{r^3} \right\rangle,$$

averaged over the unpaired electron distribution. By comparing these integrals with those of the fluorine atom, we find that the unpaired electron has approximately 18% F character, indicating a substantial degree of double bonding, in agreement with the measured bond length and bond energy and the previous work of Carrington and Howard.⁹ In future work, we will use the results presented here to help assign the observed cross-spin LMR transitions and to predict additional similar transitions, which will then yield a precise measurement of the spin-orbit coupling constant, as well as a more complete determination of the ground-state molecular parameters.

ACKNOWLEDGMENTS

R. J. S. and K. G. L. thank the National Science Foundation for support (CHE80-0704201), and K. G. L. thanks the University of California for a Regents Fellowship. We thank Dr. John Brown for substantial assistance

and encouragement with the analysis, and thank Dr. J. T. Hougen and Dr. E. Hirota for helpful criticisms of this manuscript.

- ¹J. T. Hougen, J. A. Mucha, D. A. Jennings, and K. M. Evenson, *J. Mol. Spectrosc.* **72**, 463 (1978).
- ²T. A. Dixon and R. C. Woods, *J. Chem. Phys.* **67**, 3956 (1977).
- ³F. J. Lovas and P. H. Krupenie, *J. Phys. Chem. Ref. Data* **3**, 245 (1974).
- ⁴G. R. Bird and R. C. Mockler, *Phys. Rev.* **91**, 222A (1953).
- ⁵S. Saito, Y. Endo, and E. Hirota (private communication).
- ⁶E. B. Andrews and R. F. Barrow, *Proc. Phys. Soc. London* **644**, 481 (1951).
- ⁷T. L. Porter, D. E. Mann, and N. Acquista, *J. Mol. Spectrosc.* **16**, 228 (1965).
- ⁸M. Jacox and D. E. Milligan, *J. Chem. Phys.* **50**, 3252 (1969).
- ⁹A. Carrington and B. J. Howard, *Mol. Phys.* **18**, 225 (1970).
- ¹⁰R. J. Saykally and K. M. Evenson, "The Far-Infrared Laser Magnetic Resonance Spectrum of CF," in 34th Symp. on Mol. Spectrosc., Columbus, OH, June, 1979, Paper TF-4.
- ¹¹K. Kawaguchi, C. Yamada, Y. Hamada, and E. Hirota, *J. Mol. Spectrosc.* **86**, 136 (1981).
- ¹²R. A. Frosch and H. M. Foley, *Phys. Rev.* **88**, 1337 (1952).
- ¹³J. A. Hall and W. G. Richards, *Mol. Phys.* **23**, 331 (1972).
- ¹⁴J. A. Mucha, K. M. Evenson, D. A. Jennings, G. B. Ellison, and C. J. Howard, *Chem. Phys. Lett.* **66**, 244 (1979).
- ¹⁵K. M. Evenson, R. J. Saykally, and J. T. Hougen, in 34th Symp. on Mol. Spectrosc., Columbus, OH, June, 1979, Paper TF-5.
- ¹⁶K. M. Evenson, R. J. Saykally, D. A. Jennings, R. F. Curl, and J. M. Brown, in *Chemical and Biochemical Applications of Lasers*, edited by C. B. Moore (Academic, New York, 1980), Vol. V.
- ¹⁷J. A. Mucha, D. A. Jennings, E. M. Evenson, and J. T. Hougen, *J. Mol. Spectrosc.* **72**, 463 (1978).
- ¹⁸D. J. E. Knight, NPL Report No. Qu45, Fourth Issue, March, 1978.
- ¹⁹J. M. Brown, M. Kaise, C. M. L. Kerr, and D. J. Milton, *Mol. Phys.* **36**, 553 (1978).
- ²⁰R. S. Mulliken and A. Christy, *Phys. Rev.* **38**, 87 (1931).
- ²¹R. J. Saykally, K. G. Lubic, and K. M. Evenson, *Molecular Ions: Geometric and Electronic Structures*, NATO ASI, edited by J. Berkowitz, Kos. (Dordrecht, Reidel, 1980).
- ²²A. Abragam and J. H. Van Vleck, *Phys. Rev.* **92**, 1448 (1953).
- ²³T. A. Miller, *J. Chem. Phys.* **54**, 330 (1971).
- ²⁴A. Carrington, D. H. Levy, and T. A. Miller, *Adv. Chem. Phys.* **18**, 149 (1970).
- ²⁵W. L. Meerts, *Chem. Phys.* **14**, 421 (1976).
- ²⁶T. H. Dunning, Jr., W. P. White, R. M. Pitzer, and C. W. Matthews, *J. Mol. Spectrosc.* **75**, 297 (1979).
- ²⁷R. K. Hinkley, J. A. Hall, T. E. H. Walker, and W. G. Richards, *J. Phys. B* **5**, 204 (1972).
- ²⁸J. S. M. Harvey, *Proc. R. Soc. London Ser. A* **285**, 581 (1965).
- ²⁹L. Pauling, *The Nature of The Chemical Bond*, 3rd ed. (Cornell University, Ithaca, New York, 1960).
- ³⁰K. P. Huber and G. Herzberg, *Molecular Spectra and Molecular Structure*, Vol. IV (Van Nostrand Reinhold, New York, 1979).
- ³¹*Chemical Rubber Company Handbook of Chemistry and Physics*, 54th ed., edited by R. C. Weast (CRC, Cleveland, 1973).
- ³²W. Huo, *J. Chem. Phys.* **45**, 1554 (1966).